Synthesis of Ordered Mesoporous Fe$_3$O$_4$ and γ-Fe$_2$O$_3$ with Crystalline Walls Using Post-Template Reduction/Oxidation

Feng Jiao,[†] Jean-Claude Jumas,[‡] Manfred Womes,[‡] Alan V. Chadwick,[§]
Andrew Harrison,[⊥] and Peter G. Bruce*,[†]

Contribution from the School of Chemistry and EaStChem, University of St. Andrews, St. Andrews, Fife KY16 9ST, UK, Laboratoire des Agrégats Moléculaires et Matériaux Inorganiques, UMR 5072, Université Montpellier II, CC 15, Place Eugène Bataillon, 34095, Montpellier Cedex 5, France, Centre for Materials Research, School of Physical Sciences, University of Kent, Canterbury, Kent CT2 7NR, UK, and School of Chemistry and EaStChem, University of Edinburgh, Joseph Black Building, West Mains Road, Edinburgh EH9 3JJ, UK

Received May 25, 2006; E-mail: pgb1@st-andrews.ac.uk

Abstract: Ordered mesoporous Fe$_3$O$_4$ with crystalline walls (inverse spinel structure) has been synthesized for the first time, representing to the best of our knowledge, the first synthesis of a reduced mesoporous iron oxide. Synthesis was achieved by reducing ordered mesoporous α-Fe$_2$O$_3$ (corundum structure) to Fe$_3$O$_4$ spinel then to γ-Fe$_2$O$_3$ by oxidation, while preserving the ordered mesostructure and crystalline walls throughout. Such solid/solid transformations demonstrate the stability of the mesostructure to structural phase transitions from the hexagonal close packed oxide subarray of α-Fe$_2$O$_3$ (corundum structure) to the cubic close packed subarray of Fe$_3$O$_4$ spinel and γ-Fe$_2$O$_3$. Preliminary magnetic measurements reveal that the spins in both Fe$_3$O$_4$ and γ-Fe$_2$O$_3$ are frozen at 295 K, despite the wall thickness (7 nm) being less than the lower limit for such freezing in corresponding nanoparticles ($>$8 nm).

Introduction

There is intense interest in mesoporous transition metal oxides because confining d-electrons to the thin walls between pores can endow such materials with unusual magnetic, electrical, and optical properties, whereas the high internal pore surface area can lead to new and unique catalytic properties.[1−6] However the range of mesoporous transition metal oxides that may be synthesized is limited. Mesoporous synthesis usually involves the use of a soft template (a surfactant, e.g., an alkyl amine) around which the mesoporous solid is assembled or a hard template (e.g., mesoporous silica) within the pores of which the mesoporous transition metal oxide is formed, followed by template dissolution. In both case, a solution step is required, which can limit the synthesis of mesoporous transition metal oxides to those containing transition metals in oxidation states that are stable in solution.[7] Also, if the temperature range within

which the target phase forms does not coincide with the stability range of the template, the desired phase may not be obtained.

Iron oxides are particularly important because of their use for magnetic storage, as catalysts, and as potential electrodes in lithium batteries; properties that can be enhanced significantly if the materials are formed on the nanoscale.[8−14] Ordered mesoporous Fe$_2$O$_3$ with amorphous and crystalline walls (α-Fe$_2$O$_3$, corundum structure) have been prepared in bulk and thin film form.[7,13] However, all the mesoporous iron oxides or oxyhydroxides prepared to date have been fully oxidized materials (α-Fe$_2$O$_3$ and α-FeOOH), i.e., containing only Fe in the +3 oxidation state, in part because of the difficult in stabilizing lower oxidation states in solution and during synthesis.[7,13−16] The synthesis of reduced iron oxides, especially Fe$_3$O$_4$ (inverse spinel structure), is acknowledged to be an important goal.[7,17−19] Here we take ordered mesoporous Fe$_2$O$_3$

[†] University of St Andrews.
[‡] University of Montpellier.
[§] University of Kent.
[⊥] University of Edinburgh.

(1) Antonelli, D. M.; Ying, J. Y. *Angew. Chem.*, *Int. Ed. Engl.* **1995**, *34*, 2014.
(2) Schüth, F. *Chem. Mater.* **2001**, *13*, 3184.
(3) Yang, P.; Deng, T.; Zhao, D.; Feng, P.; Pine, D.; Chmelka, B. F.; Whitesides, G. M.; Stucky, G. D. *Science* **1998**, *282*, 2244.
(4) He, X.; Antonelli, D. *Angew. Chem., Int. Ed.* **2002**, *41*, 214.
(5) Behrens, P. *Angew. Chem., Int. Ed. Engl.* **1996**, *35*, 515.
(6) Huo, Q. S.; Margolese, D. I.; Ciesla, U.; Demuth, D. G.; Feng, P. Y.; Gier, T. E.; Sieger, P.; Firouzi, A.; Chmelka, B. F.; Schuth, F.; Stucky, G. D. *Chem. Mater.* **1994**, *6*, 1176.
(7) Brezesinski, T.; Groenewolt, M.; Antonietti, M.; Smarsly, B. *Angew. Chem., Int. Ed.* **2006**, *45*, 781.

(8) Arico, A. S.; Bruce, P.; Scrosati, B.; Tarascon, J. M.; Van Schalkwijk, W. *Nat. Mater.* **2005**, *4*, 366.
(9) Bruce, P. G. *Solid State Sci.* **2005**, *7*, 1456.
(10) Jiao, F.; Yue, B.; Zhu, K. K.; Zhao, D. Y.; He, H. Y. *Chem. Lett.* **2003**, *32*, 770.
(11) Larcher, D.; Masquelier, C.; Bonnin, D.; Chabre, Y.; Masson, V.; Leriche, J. B.; Tarascon, J. M. *J. Electrochem. Soc.* **2003**, *150*, A133.
(12) Ziolo, R. F.; Giannelis, E. P.; Weinstein, B. A.; Ohoro, M. P.; Ganguly, B. N.; Mehrotra, V.; Russell, M. W.; Huffman, D. R. *Science* **1992**, *257*, 219.
(13) Jiao, F.; Bruce, P. G. *Angew. Chem., Int. Ed.* **2004**, *43*, 5958.
(14) Srivastava, D. N.; Perkas, N.; Gedanken, A.; Felner, I. *J. Phys. Chem. B* **2002**, *106*, 1878.
(15) Wirnsberger, G.; Gatterer, K.; Fritzer, H. P.; Grogger, W.; Pillep, B.; Behrens, P.; Hansen, M. F.; Koch, C. B. *Chem. Mater.* **2001**, *13*, 1453.
(16) Wirnsberger, G.; Gatterer, K.; Fritzer, H. P.; Grogger, W.; Pillep, B.; Behrens, P.; Hansen, M. F.; Koch, C. B. *Chem. Mater.* **2001**, *13*, 1467.
(17) Mandernack, K. W.; Bazylinski, D. A.; Shanks, W. C.; Bullen, T. D. *Science* **1999**, *285*, 1892.

with crystalline walls (α-Fe$_2$O$_3$), convert it to ordered mesoporous Fe$_3$O$_4$ (inverse spinel structure) by reduction, then to ordered mesoporous Fe$_2$O$_3$ (γ-Fe$_2$O$_3$ structure) by oxidation, while retaining the same ordered mesostructure and with crystalline walls throughout. To our knowledge this represents the first synthesis of the important reduced mesoporous iron oxide, Fe$_3$O$_4$, indeed the first synthesis of any reduced mesoporous iron oxide. Preliminary magnetic characterization of mesoporous Fe$_3$O$_4$ and γ-Fe$_2$O$_3$ with crystalline walls is presented. Conversion of the α-Fe$_2$O$_3$ structure to Fe$_3$O$_4$ spinel involves a change from a hexagonal close-packed oxide ion array (α-Fe$_2$O$_3$) to a cubic close-packed array (Fe$_3$O$_4$). This is not a topotactic phase change; it involves sheaving of the oxide ion planes from AB to ABC stacking; yet this significant structural change can occur without destroying the ordered mesostructure. Synthesis of disordered mesoporous γ-Fe$_2$O$_3$ as a thin film phase by electrochemical means has been reported recently.[20]

The synthesis of mesoporous transition metal oxides has proved a formidable challenge, however, a challenge that has seen important advances in recent years.[1–6,13,21–22] The recent advent of hard templating methods represents a major milestone.[23–34] Here we use the hard templating method, details of which are described below.

Experiment Section

Three-dimensional mesoporous silica (KIT-6) with *Ia-3d* symmetry was used as hard template. The synthesis of mesoporous KIT-6 has been described in previous reports.[35,36] In a typical synthesis of mesoporous Fe$_3$O$_4$: 1 g of Fe(NO$_3$)$_3$·9H$_2$O (98%, Aldrich) was dissolved in 20 mL of ethanol, followed by addition of 1 g of mesoporous silica, KIT-6. After stirring at room temperature until all the solution had been absorbed and a dry powder obtained, the sample was heated slowly to 600 °C in air and calcined at that temperature for 6 h. The resulting sample was twice treated with a hot 2 M NaOH solution to remove the silica template, followed by washing with water and ethanol several times, and then drying at 60 °C. This procedure leads to mesoporous α-Fe$_2$O$_3$ with crystalline walls as described in reference 33. Reduction was achieved by heating at 350 °C for 1 h under a 5% H$_2$–95% Ar atmosphere. Mesoporous Fe$_3$O$_4$ was stored
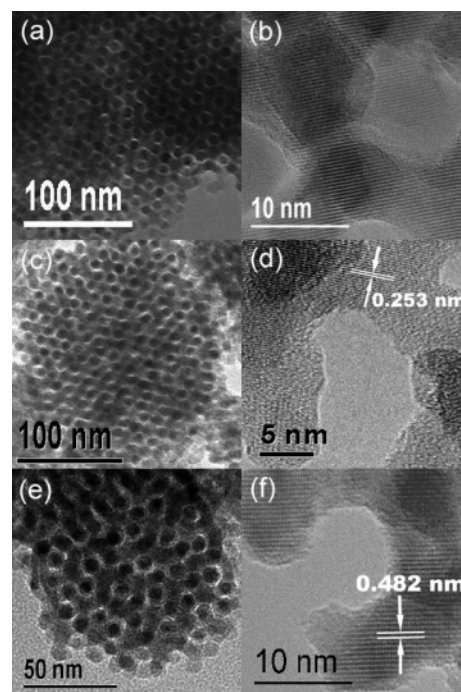

Figure 1. TEM images recorded along the [111] direction for mesoporous (a) α-Fe$_2$O$_3$, (c) Fe$_3$O$_4$, and (e) γ-Fe$_2$O$_3$; HRTEM images for mesoporous (b) α-Fe$_2$O$_3$, (d) Fe$_3$O$_4$, and (f) γ-Fe$_2$O$_3$.

under Ar, and all structure characterization was carried out without exposure to air. For the preparation of mesoporous γ-Fe$_2$O$_3$, the as-prepared mesoporous Fe$_3$O$_4$ was heated at 150 °C for 2 h in air.

The materials were characterized by transmission electron microscopy (TEM, Jeol JEM-2011), powder X-ray diffraction (PXRD, Stoe STADI/P diffractometer operating in transmission mode with Fe$_{K\alpha1}$ radiation, $\lambda = 1.936$ Å), Low angle X-ray diffraction (Rigaku/MSC, D/max-rB with Cu$_{K\alpha1}$ radiation, $\lambda = 1.541$ Å) and N$_2$ adsorption (Hiden IGA porosimeter). ^{57}Fe Mössbauer spectra were recorded in transmission geometry on a standard EG&G spectrometer in the constant acceleration mode, using a ^{57}Co(Rh) source. Magnetization measurements were made on a Quantum Design MPMS$_2$ SQUID magnetometer in a field of 0.01 T.

Results and Discussion

The highly ordered mesostructures of α-Fe$_2$O$_3$, Fe$_3$O$_4$, and γ-Fe$_2$O$_3$ are evident in Figure 1, a, c, and e. Although the synthesis of ordered mesoporous α-Fe$_2$O$_3$ using KIT-6 and its characterization by TEM, PXRD, and N$_2$ adsorption−desorption have been reported previously, the TEM data are included here to demonstrate retention of the mesoporous structure during the reduction and oxidation.[33] For all three mesoporous materials the symmetry is that anticipated for a replica of the KIT-6 template structure (*Ia-3d*). The a_o parameters extracted from the TEM data are 23.2 nm (α-Fe$_2$O$_3$), 24.4 nm (Fe$_3$O$_4$) and 23.0 nm (γ-Fe$_2$O$_3$). These data indicate that the mesostructure is maintained throughout the reduction and oxidation with only a slight expansion on conversion from α-Fe$_2$O$_3$ to Fe$_3$O$_4$ and contraction on transformation from Fe$_3$O$_4$ to γ-Fe$_2$O$_3$. The high-resolution TEM (HRTEM) images in Figures 1b, d and f show the detailed structure of the mesopores. The ordered mesostructures and pore shapes of α-Fe$_2$O$_3$, Fe$_3$O$_4$, and γ-Fe$_2$O$_3$ seen in Figure 1 are typical of those observed throughout the materials, based on examining many different regions and many particles. The results of low-angle powder X-ray diffraction data

(18) Bazylinski, D. A.; Heywood, B. R.; Mann, S.; Frankel, R. B. *Nature* **1993**, *366*, 218.
(19) Ozdemir, O.; Dunlop, D. J. *Science* **1989**, *243*, 1043.
(20) Shi, K. Y.; Peng, L. M.; Chen, Q.; Wang, R. H.; Zhou, W. Z. *Microporous Mesoporous Mater.* **2005**, *83*, 219.
(21) Tian, Z. R.; Tong, W.; Wang, J. Y.; Duan, N. G.; Krishnan, V. V.; Suib, S. L. *Science* **1997**, *276*, 926.
(22) Yang, P.; Zhao, D.; Margolese, D. I.; Chmelka, B. F.; Stucky, G. D. *Nature* **1998**, *396*, 152.
(23) Yang, H. F.; Zhao, D. Y. *J. Mater. Chem.* **2005**, *15*, 1217.
(24) Lee, J.; Han, S.; Hyeon, T. *J. Mater. Chem.* **2004**, *14*, 478.
(25) Kleitz, F.; Choi, S. H.; Ryoo, R. *Chem. Commun.* **2003**, 2136.
(26) Laha, S. C.; Ryoo, R. *Chem. Commun.* **2003**, 2138.
(27) Tian, B. Z.; Liu, X. Y.; Yang, H. F.; Xie, S. H.; Yu, C. Z.; Tu, B.; Zhao, D. Y. *Adv. Mater.* **2003**, *15*, 1370.
(28) Crepaldi, E. L.; Soler-Illia, G.; Grosso, D.; Cagnol, F.; Ribot, F.; Sanchez, C. *J. Am. Chem. Soc.* **2003**, *125*, 9770.
(29) Li, W. C.; Lu, A. H.; Weidenthaler, C.; Schuth, F. *Chem. Mater.* **2004**, *16*, 5676.
(30) Zhu, K. K.; Yue, B.; Zhou, W. Z.; He, H. Y. *Chem. Commun.* **2003**, 98.
(31) Tian, B. Z.; Liu, X. Y.; Solovyov, L. A.; Liu, Z.; Yang, H. F.; Zhang, Z. D.; Xie, S. H.; Zhang, F. Q.; Tu, B.; Yu, C. Z.; Terasaki, O.; Zhao, D. Y. *J. Am. Chem. Soc.* **2004**, *126*, 865.
(32) Wang, Y. Q.; Yang, C. M.; Schmidt, W.; Spliethoff, B.; Bill, E.; Schuth, F. *Adv. Mater.* **2005**, *17*, 53.
(33) Jiao, F.; Harrison, A.; Jumas, J. C.; Chadwick, A. V.; Kockelmann, W.; Bruce, P. G. *J. Am. Chem. Soc.* **2006**, *128*, 5468.
(34) Jiao, F.; Shaju, K. M.; Bruce, P. G. *Angew. Chem., Int. Ed.* **2005**, *44*, 6550.
(35) Kleitz, F.; Choi, S. H.; Ryoo, R. *Chem. Commun.* **2003**, *17*, 2136.
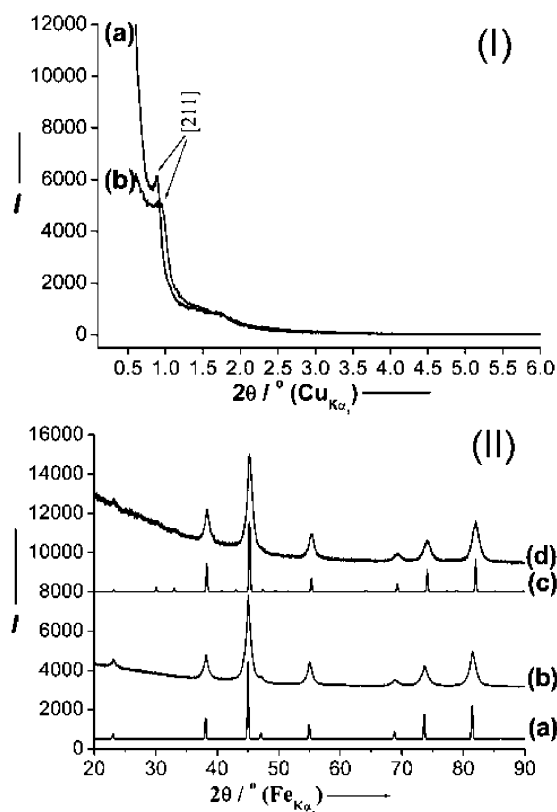(36) Kim, T. W.; Kleitz, F.; Paul, B.; Ryoo, R. *J. Am. Chem. Soc.* **2005**, *127*, 7601.

Figure 2. (I) Low-angle PXRD patterns for mesoporous (a) Fe$_3$O$_4$ and (b) γ-Fe$_2$O$_3$; (II) wide-angle PXRD patterns for (a) bulk Fe$_3$O$_4$, (b) mesoporous Fe$_3$O$_4$, (c) bulk γ-Fe$_2$O$_3$ and (d) mesoporous γ-Fe$_2$O$_3$.

Figure 3. (a) N$_2$ adsorption−desorption isotherms and (b) pore size distribution for mesoporous γ-Fe$_2$O$_3$.

for Fe$_3$O$_4$ and γ-Fe$_2$O$_3$ are shown in Figure 2(I), a and b. Both materials exhibit a peak around 0.9° in 2θ assigned to [211] reflection, with a weaker secondary peak at about 1.7° (CuKα$_1$). From the low angle [211] reflection, the a_o parameters for Fe$_3$O$_4$ and γ-Fe$_2$O$_3$ were determined to be 24.5 and 23.4 nm respectively, values that are in good agreement with those obtained from the TEM data in Figure 1.

The above results demonstrate that mesoporous α-Fe$_2$O$_3$ can convert to Fe$_3$O$_4$ then to γ-Fe$_2$O$_3$ with retention of the mesostructure. The ability to carry out solid/solid transformations in mesoporous solids, and with retention of the mesostructure, has been observed previously: for example, transformation of ordered mesoporous Co$_3$O$_4$ with the spinel structure, to the spinel-based low-temperature LiCoO$_2$ (Li$_2$-Co$_2$O$_4$), by reacting mesoporous Co$_3$O$_4$ with LiOH at 400 °C.[34] In another case, mesoporous goethite (α-FeOOH) has been transformed to hematite (α-Fe$_2$O$_3$) by heating at 450 °C.[7] However, in both cases, the oxygen subarray retains the same close packing, ccp in the case of the spinel−spinel transformation and hcp in the case of goethite to hemeatite transformation, whereas here the more difficult conversion from hcp to ccp, involving the sheaving of oxygen layers, from AB to ABC stacking, occurs. The thin walls endow the mesoporous solids with a flexibility that aids such solid/solid transformations while preserving the mesostructure.

N$_2$ sorption isotherms were collected for γ-Fe$_2$O$_3$ and are presented in Figure 3a. Because mesoporous Fe$_3$O$_4$ converts to the γ-phase on exposure to air, it was not possible to obtain reliable sorption isotherms for Fe$_3$O$_4$. The data for γ-Fe$_2$O$_3$ exhibit a type-IV isotherm, typical of a mesoporous transition
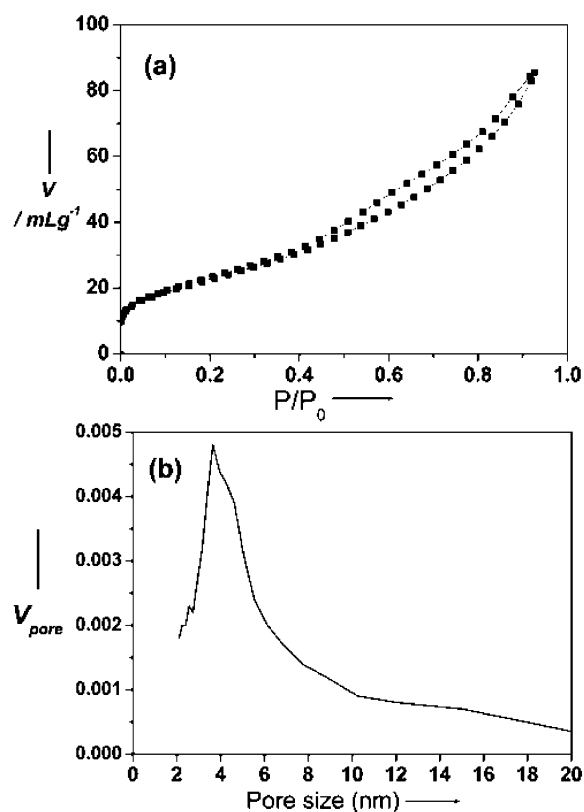
metal oxide prepared by the hard-templating method.[32,33] The pore size distribution is shown in Figure 3b. The peak is centered around 3.6 nm, which is in good agreement with the value expected for a replica of the KIT-6 structure.[33,34] The Brunauer−Emmett−Teller (BET) surface area for mesoporous γ-Fe$_2$O$_3$ is 86 m^2 g^{-1}.

Turning to the structures of the walls, it is evident from the wide-angle powder X-ray diffraction data, Figure 2(II) b and d, that the walls are highly crystalline; the PXRD data exhibit well-defined peaks corresponding to the crystal structures of Fe$_3$O$_4$ [Figure 2(II)b] and γ-Fe$_2$O$_3$ [Figure 2(II)d]. Although the diffraction patterns look similar for both compounds, they are different with different space groups (*Fd3*m and *P*4$_3$32 for Fe$_3$O$_4$ and γ-Fe$_2$O$_3$, respectively) and lattice parameters that differ significantly (8.385 Å and 8.346 Å for Fe$_3$O$_4$ and γ-Fe$_2$O$_3$, respectively, JCPDS Nos. 19-629 and 25-1402). Refinement using the Rietveld method yielded cubic lattice parameters of 8.383(2) Å (Fe$_3$O$_4$) and 8.343(2) Å (γ-Fe$_2$O$_3$) for the mesoporous materials, in excellent agreement with literature values. These results demonstrate that Fe$_3$O$_4$ spinel has been successfully synthesized and converted to γ-Fe$_2$O$_3$; further corroboration of the Fe$_3$O$_4$ formation and conversion to γ-Fe$_2$O$_3$ has been obtained from EXAFS/XANES and is discussed later. Although the PXRD data indicate that the walls are highly crystalline, examination of the HRTEM images in Figure 1, d and f, shows that each particle is not a single crystal; instead, the lattice fringes run in different directions in different regions of the particles. Lattice fringe spacings of 2.53 and 4.82 Å are highlighted in Figure 1, d and f, and correspond well with the d spacings of the [311] and [113] reflections for Fe$_3$O$_4$ and γ-Fe$_2$O$_3$, respectively, in agreement with the values of 2.532

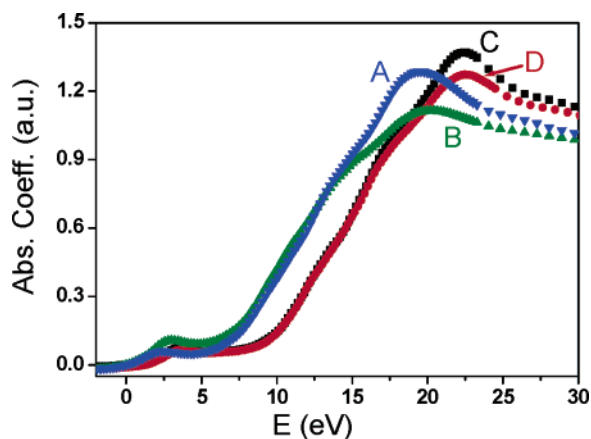**Figure 4.** XANES data for (A) bulk Fe_3O_4 (blue line), (B) mesoporous Fe_3O_4 (green line), (C) bulk γ-Fe_2O_3 (black line), and (D) mesoporous γ-Fe_2O_3 (red line).

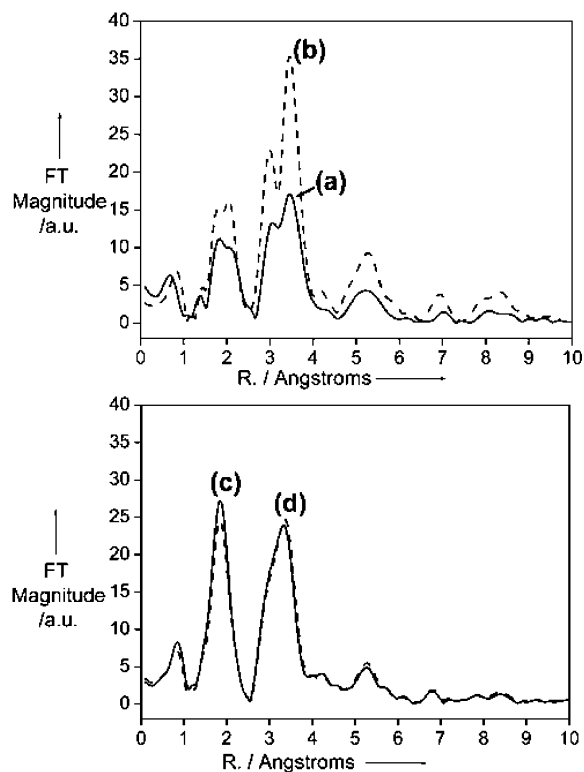**Figure 5.** EXAFS results for (a) mesoporous Fe_3O_4 (solid line), (b) bulk Fe_3O_4 (dash line), (c) mesoporous γ-Fe_2O_3 (solid line), and (d) bulk γ-Fe_2O_3 (dashed line).

and 4.82 Å obtained from the JCPDS database (JCPDS Nos. 19-629 and 25-1402).

Further confirmation that mesoporous compound with the composition Fe_3O_4 has been prepared and then converted to γ-Fe_2O_3 was obtained from EXAFS/XANES. The Fe L_m XANES of mesoporous Fe_3O_4 and γ-Fe_2O_3 are presented in Figure 4, after the smooth preedge background subtraction and normalization. The XANES data for the bulk materials are also shown for comparison. It is clear that mesoporous Fe_3O_4 and γ-Fe_2O_3 have average oxidation states of +2.66 and +3, respectively. The Fourier transformed EXAFS data are presented in Figure 5 along with data for the corresponding bulk phases (raw data deposited). The data for the mesoporous and corresponding bulk materials are identical, confirming the results
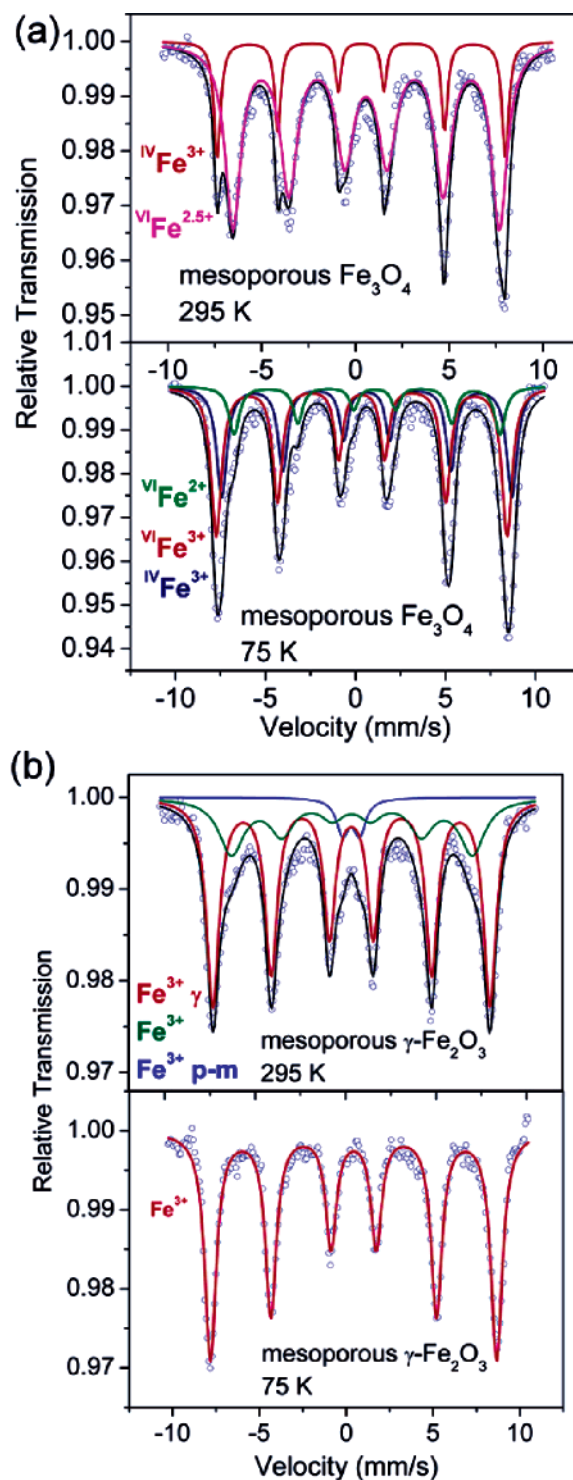
Figure 6. Mössbauer data recorded at 295 and 75 K for mesoporous (a) Fe_3O_4 and (b) γ-Fe_2O_3 (open circles: experimental data; solid black line: best fit).

from the powder X-ray diffraction measurements. The differences between the spectra for Fe_3O_4 and γ-Fe_2O_3 further confirm that the two different forms of iron oxide have been prepared.

Mössbauer data are presented in Figure 6 for mesoporous Fe_3O_4 and γ-Fe_2O_3 at 75 and 295 K. The data for Fe_3O_4, inverse spinel ($Fe_{tet}^{3+}[Fe^{2+}Fe^{3+}]_{oct}O_4$) at 295 K are composed of two sextuplets, one corresponding to the tetrahedral site Fe^{3+} ion and the other to an average oxidation state of $Fe^{2.5+}$ in an octahedral site (Figure 6a). The latter is consistent with electron
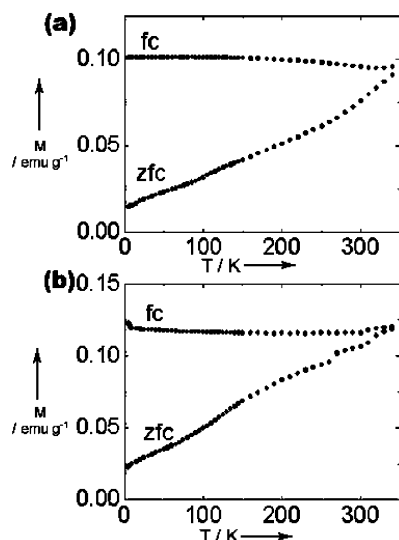
Figure 7. Magnetization measured after cooling in zero field (zfc) and then in a field of 0.01 T (fc) for mesoporous (a) Fe_3O_4 and (b) γ-Fe_2O_3.

exchange between the high-spin Fe^{2+} and Fe^{3+} ions in the 16d octahedral sites of the *Fd3m* spinel structure being sufficiently rapid, on the time scale of the Mössbauer experiment, to ensure that the individual iron ions are indistinguishable. Bulk magnetite undergoes the characteristic Verwey transition in the region of 120 K, manifested most distinctively by a metal−insulator transition on cooling. The traditional rationalization of this transition involves a localization and ordering of charge on the Fe^{2+} and Fe^{3+} ions of the octahedral sites in the low-temperature state, although there is still considerable debate about this.[37,38] Data taken at 75 K on mesoporous Fe_3O_4 are compatible with such charge ordering: three sextuplets may be distinguished, corresponding to tetrahedral Fe^{3+}, octahedral Fe^{3+}, and octahedral Fe^{2+} (Figure 6a). At both temperatures the Mössbauer data are consistent with magnetic ordering. The magnetization data (Figure 7a) are also consistent with this conclusion: a divergence in field-cooled (fc) and zero-field-cooled (zfc) data indicate that spin freezing has occurred at the highest experimental temperature of 340 K (bulk Fe_3O_4 undergoes a paramagnetic-to-ferromagnetic transition around 850 K). The Verwey transition is sometimes manifested in Fe_3O_4 as an anomaly in the magnetization, but we see no sign of such a feature; however this can, in some cases, be difficult to detect by dc magnetization.[39−41]

Considering the Mössbauer data for γ-Fe_2O_3 and beginning with the data at 75 K, these data may be fitted by a single sextuplet (Figure 6b). The literature on bulk γ-Fe_2O_3 indicates that, although Fe^{3+} is present on both the tetrahedral and the octahedral sites of the spinel structure, the sextuplets of both sites overlap significantly, consistent with our observations at low temperatures for mesoporous γ-Fe_2O_3. At room temperature, the spectrum is again dominated by a sextuplet of Fe^{3+}, in accord with the bulk material (Figure 6b, labeled Fe^{3+} γ). However, there are two other contributions from Fe^{3+} to the data for mesoporous γ-Fe_2O_3 at room temperature, a sextuplet of much

lower intensity (labeled Fe^{3+}) and a weak doublet corresponding to paramagnetic Fe^{3+} (Fe^{3+} p-m). At both temperatures the Mössbauer data are consistent with magnetic order. Fe^{2+} and Fe^{3+} are formal valence state, which does not mean that the charge states are exactly 2.00 and 3.00 in agreement with Wright's previous report.[38] The magnetization data under zfc and fc conditions (Figure 7b) indicate that spin freezing has occurred by 340 K and are broadly consistent with data for bulk samples (magnetic ordering occurs in bulk γ-Fe_2O_3 below approximately 900 K); they are also compatible with magnetic order.

Further work is required to characterize the magnetic structures of mesoporous Fe_3O_4 and γ-Fe_2O_3 in more detail. Such work is underway, addressing in particular the absence of the Verwey transition signature in the dc magnetization measurements for Fe_3O_4 and to fully understand the various contributions to the Mössbauer data for γ-Fe_2O_3 at room temperature. However, it is clear that mesoporous Fe_3O_4 and γ-Fe_2O_3 exhibit magnetic order. These results are in accord with our recent observations of magnetic ordering in mesoporous α-Fe_2O_3 with crystalline walls. In that case, long-range magnetic ordering was observed for a wall thickness of approximately 7 nm, despite the fact that nanoparticles of dimensions less than 8 nm exhibit a breakdown of magnetic order and superparamagnetic behavior.[33] The magnetic interactions along the 2D walls are sufficient to promote magnetic order. We suggest that a similar mechanism may explain the observations of magnetic freezing in mesoporous Fe_3O_4 and γ-Fe_2O_3; such freezing is absent in nanoparticles of these phases at such temperatures if less than 8 nm in diameter.[42,43] The retention of magnetic order at relatively high temperatures in mesoporous Fe_3O_4 and γ-Fe_2O_3 may be significant for technological applications.

Conclusions

Mesoporous Fe_3O_4 has been synthesized. This is the first synthesis of mesoporous Fe_3O_4 or any reduced mesoporous iron oxide, something that is difficult to carry out directly. Starting from ordered mesoporous α-Fe_2O_3 with crystalline walls, reduction results in the formation of Fe_3O_4, and then oxidation yields γ-Fe_2O_3, while preserving the same ordered mesostructure and crystalline walls throughout these solid/solid transformations, emphasizing the flexibility of mesoporous solids to such transformations. The magnetic properties of mesoporous Fe_3O_4 and γ-Fe_2O_3 have been characterized by Mössbauer and SQUID measurements. The materials exhibit magnetic freezing above 340 K despite wall thicknesses of ∼7 nm, whereas nanoparticles of the corresponding iron oxides lose magnetic order below a particle size of 8 nm down to much lower temperatures.

(37) Garcia, J.; Subias, G. *J. Phys.:Condens. Matter* **2004**, *16*, R145.
(38) Wright, J. P.; Attfield, J. P.; Radaelli, P. G. *Phys. Rev. B* **2002**, *66*, 214422.
(39) Goya, G. F.; Berquo, T. S.; Fonseca, F. C.; Morales, M. P. *J. Appl. Phys.* **2003**, *94*, 3520.
(40) Sena, S. P.; Lindley, R. A.; Blythe, H. J.; Sauer, C.; Al-Kafarji, M.; Gehring, G. A. *J. Magn. Magn. Mater.* **1997**, *176*, 111.
(41) Chapline, M. G.; Wang, S. X. *J. Appl. Phys.* **2005**, *97*, 123901.

(42) Yang, T. Z.; Shen, C. M.; Li, Z.; Zhang, H. R.; Xiao, C. W.; Chen, S. T.; Xu, Z. C.; Shi, D. X.; Li, J. Q.; Gao, H. J. *J. Phys. Chem. B* **2005**, *109*, 23233.
(43) Tartaj, P.; Gonzalez-Carreno, T.; Serna, C. J. *J. Phys. Chem. B* **2003**, *107*, 20.